JOURNAL OF SPACECRAFT AND ROCKETS
Vol. 35, No. 3, May–June 1998

Entry Guidance for the X-33 Vehicle

Ping Lu*
Iowa State University, Ames, Iowa 50011-3231
and
John M. Hanson†
NASA Marshall Space Flight Center, Alabama 35812

The entry flight of the X-33 Advanced Technology Demonstrator is first examined by using a trajectory optimization approach. For closed-loop guidance the nominal entry trajectory is defined by a piecewise linear drag vs an energy profile. Under a nonlinear tracking control law and an onboard drag-profile updating scheme, the vehicle reaches the designated target point accurately. To further meet the stringent heading requirement at this point, a ground-track design method and the corresponding trajectory control law, which can be applied at a distance before the vehicle reaches the target point, are developed. Simulations with the X-33 vehicle and trajectory data demonstrate good performance of the guidance algorithms.

Nomenclature

C_L, C_D = lift and drag coefficients, respectively
D = nondimensional drag acceleration, g
e = nondimensional specific energy
g_0 = gravitational acceleration, 9.81 m/s^2
L = nondimensional lift acceleration, g
$n_{z\max}$ = maximum allowable normal acceleration, g
$\dot{Q}_s$, $\dot{Q}_{\max}$ = nondimensional heat rate at stagnation point and its maximum allowable value
$\bar{q}$, $\bar{q}_{\max}$ = nondimensional dynamic pressure and its maximum allowable value
R_0 = radius of Earth, 6,378,145 m
r = radial distance from Earth's center to the vehicle, normalized by R_0
s = downrange distance normalized by R_0
s_f = required value for s
t = time, s
u = $C_L \cos\sigma / C_D$
V = Earth-relative velocity, normalized by $\sqrt{(g_0 R_0)}$
α = angle of attack, rad
α_{ref} = nominal for α, scheduled with respect to V
γ = flight-path angle, rad
ζ, ζ_F = damping ratios
θ = longitude, rad
σ = bank angle, rad
τ = nondimensional time $t/\sqrt{(R_0/g_0)}$
ϕ = latitude, rad
ψ = velocity azimuth angle, rad
Ω = self-rotation rate of Earth, normalized by $\sqrt{(g_0/R_0)}$
ω, ω_{n_F} = natural frequencies normalized by $\sqrt{(g_0/R_0)}$

Introduction

THE X-33 Advanced Technology Demonstrator is a half-scale prototype developed to test the technologies needed for the full-scale single-stage reusable launch vehicle (RLV). In the test flights projected to begin in 1999, the vehicle will be launched vertically from Edwards Air Force Base in California and accelerate up to a maximum velocity of about Mach 14. The vehicle will land horizontally at one of several potential sites in California, Utah, or Montana, depending on the velocity of the vehicle at the main engine cutoff (MECO). The entry guidance is concerned with guiding the vehicle from (or a short period after) MECO, or from atmospheric penetration in the case of the full-scale RLV, to the landing site while satisfying a number of in flight constraints and providing appropriate conditions at the handover to the terminal area energy management (TAEM) for final approach and landing. The basic entry guidance concept for the X-33 will follow that for the Space Shuttle[1] in that the vehicle will track a nominal drag acceleration profile. However, there are significant differences, one of which is to schedule the entire drag profile as a function of the specific energy.[2] In Ref. 3, it has been shown that, when the drag profile is defined to be a piecewise linear function of the energy, such a parameterization gives rise to an accurate analytical prediction of the downrange distance along the nominal trajectory. This approach very efficiently produces a nominal drag profile subject to various in flight constraints and the downrange distance requirement, thus allowing quick tradeoff studies and planning of the entry trajectory for a lifting vehicle returning from orbit.

The X-33 will be a suborbital vehicle, and its entry flight will have several unique features that are not shared by the entry trajectory of an orbital vehicle. An orbital vehicle can choose the most convenient deorbit point and the desired entry flight-path angle. For the X-33, entry is directly tied to ascent; thus, the design of the point-to-point entry trajectory for the X-33 is more difficult. Before its descent begins, the X-33 will continue to ascend after MECO because of the positive flight-path angle at MECO. The maximum velocity during the flight tests of the X-33 will be about Mach 14 instead of Mach 25 for an orbital vehicle. In addition, early specifications on some of the flight tests of the X-33 place stringent heading requirements at the TAEM point that are not common in entry flight of an orbital vehicle.

This paper investigates an entry guidance scheme for the X-33. First, the nominal entry trajectories are obtained by solving a complex trajectory optimization problem using full three-dimensional equations of motion. Although computationally intensive, these solutions provide necessary understanding of the X-33 entry flight and serve as the benchmarks for the entry trajectory design. Next, the approach in Ref. 3 is shown to produce a very similar drag profile as the one along the optimal trajectory, but much more efficiently and quickly. Under a nonlinear drag-profile tracking control law and an onboard drag-profile updating scheme, the vehicle reaches the designated TAEM point accurately. To further meet stringent heading requirements at the TAEM point, a ground-track design method and the corresponding trajectory control law, which can be applied near TAEM, have been developed. Simulations with the X-33 vehicle and trajectory data demonstrate good performance of the guidance algorithms.

Note that, although the MECO and TAEM data as well as the X-33 vehicle data used in this paper are from early X-33 trajectory and vehicle designs, this study is an independent effort that does not

Received Aug. 11, 1997; revision received Jan. 12, 1998; accepted for publication Jan. 26, 1998.

*Associate Professor, Department of Aerospace Engineering and Engineering Mechanics. E-mail: plu@iastate.edu. Associate Fellow AIAA.

†Chief, Flight Mechanics, Guidance, Navigation, and Control Systems Branch, Mail Code ED13.

mean to represent the actual X-33 trajectory design and guidance algorithms.

Optimal Three-Dimensional Entry Trajectories

Formulation

We begin with the point-mass dimensionless equations of three-dimensional motion over a spherical rotating Earth[4]:

$$\dot{r} = V \sin\gamma \tag{1}$$

$$\dot{\theta} = \frac{V \cos\gamma \sin\psi}{r \cos\phi} \tag{2}$$

$$\dot{\phi} = \frac{V \cos\gamma \cos\psi}{r} \tag{3}$$

$$\dot{V} = -D - (\sin\gamma / r^2) + \Omega^2 r \cos\phi(\sin\gamma \cos\phi - \cos\gamma \sin\phi \cos\psi) \tag{4}$$

$$\dot{\gamma} = (1/V)\{L\cos\sigma + [V^2 - (1/r)](\cos\gamma/r) + 2\Omega V \cos\phi \sin\psi + \Omega^2 r \cos\phi(\cos\gamma \cos\phi + \sin\gamma \cos\psi \sin\phi)\} \tag{5}$$

$$\dot{\psi} = \frac{1}{V}\left[\frac{L\sin\sigma}{\cos\gamma} + \frac{V^2}{r}\cos\gamma \sin\psi \tan\phi - 2\Omega V \times (\tan\gamma \cos\psi \cos\phi - \sin\phi) + \frac{\Omega^2 r}{\cos\gamma}\sin\psi \sin\phi \cos\phi\right] \tag{6}$$

where the velocity azimuth angle ψ is measured from the north in a clockwise direction. The differentiation is with respect to the dimensionless time τ. The main reason for using the dimensionless form is better numerical conditioning of the trajectory optimization problem discussed subsequently.

We assume that the entry begins immediately after MECO. The conditions at MECO, determined by the ascent trajectory, are given. The terminal conditions of the X-33 entry trajectory are specified by TAEM requirements. They are results of tradeoff studies combining entry and TAEM maneuvers and are given explicitly as

$$r(\tau_f) = r_f, \qquad \theta(\tau_f) = \theta_f, \qquad \phi(\tau_f) = \phi_f$$
$$V(\tau_f) = V_f, \qquad \gamma_{\min} \le \gamma(\tau_f) \le \gamma_{\max}, \qquad \psi(\tau_f) = \psi_f \tag{7}$$

where r_f is at an altitude of about 24–25 km (80,000 ft) and V_f corresponds to about 745 m/s (Mach 2.5); θ_f and ϕ_f are determined by the landing site; and the typical γ_f is between -11 and -15 deg. The velocity azimuth ψ_f is determined by the TAEM maneuvers and other operational considerations. In addition, the following trajectory constraints are imposed:

$$|L\cos\alpha + D\sin\alpha| \le n_{z_{\max}} \tag{8}$$

$$\bar{q} \le \bar{q}_{\max} \tag{9}$$

$$\dot{Q}_s \le \dot{Q}_{\max} \tag{10}$$

$$[(1/r) - V^2](1/r) - L \le 0 \tag{11}$$

where Eq. (8) is a constraint on the acceleration in the body-normal direction, Eq. (9) is on dynamic pressure $\bar{q}$, and Eq. (10) is on heat rate $\dot{Q}_s$ at a stagnation point. Multiple heat-rate constraints for several stagnation points can be imposed, although only one is used in this work. In this study, $n_{z_{\max}} = 2.5\ g$, $\bar{q}_{\max} = 11{,}970\ \text{N/m}^2$ (250 psf), and $\dot{Q}_{\max} = 431{,}259\ \text{W/m}^2$ (38 Btu/s-ft^2) are used. The last constraint (11) is called the equilibrium glide constraint, obtained by setting $\gamma = \dot{\gamma} = 0$ in Eq. (5) with $\sigma = 0$ and neglecting Ω, although other nonzero constant σ and γ also may be used to achieve equilibrium glide. Such a constraint is useful in reducing the altitude oscillation along the entry trajectory for an orbital vehicle.[1] For the X-33, this constraint is not as critical, particularly for short-range entry flight. Nonetheless, it is still retained here because it provides a convenient lower bound on the drag acceleration that will be used later.

In the following design of the nominal entry trajectory, the angle of attack α is scheduled as a function of velocity, beginning at large value (40 deg at 4000 m/s and above) and gradually reducing to 8 deg at the TAEM point. The bank angle σ is modulated to control the trajectory. Therefore, in this section, σ is parameterized as a piecewise linear function of time. The nodal values of the parameterization of σ and the flight time τ_f are found to satisfy the TAEM condition (7) and the inflight constraints (8–11) and to minimize a performance index

$$J = \int_0^{\tau_f} \sqrt{\rho} V^3 \, d\tau \tag{12}$$

where $\rho = 1.752 e^{-R_0(r-1)/6700}\ \text{kg/m}^3$ is a reasonably good approximation to the 1976 U.S. Standard Atmosphere in the altitude range of interest to entry flight.[5] The performance index (12) is proportional to the accumulated heat load per unit area at the stagnation point. Note here that other performance indices, such as

$$J = \int_0^{\tau_f} \rho V^3 \, d\tau \tag{13}$$

also may be used. In this case the integrand in Eq. (13) is proportional to the average heat rate on the surface of the vehicle, and the performance index is thus proportional to the total heat load of the vehicle. We have found that the choice of different performance indices has relatively minor effect on the final trajectory. This is because the trajectory is already tightly constrained by the TAEM conditions and constraints (8–11); therefore, little room is available for significant optimization of any performance index. A performance index mostly serves to facilitate the search for a feasible trajectory using an optimization algorithm. For comparison of the results obtained later from piecewise linear drag profiles, which use Eq. (12) as the performance index, we use Eq. (12) in the numerical solutions.

Numerical Solutions

To solve the parameter optimization problem using a nonlinear programming algorithm, each of the constraints (8–11), represented by $p_i(\tau) \le 0, \forall \tau \in [0, \tau_f]$, $i = 1, \ldots, 4$, is converted into a terminal inequality constraint by

$$w_i(\tau_f) \le 0, \quad \text{where} \quad \dot{w}_i = \max\{\delta, p_i\} \quad \text{and} \quad w_i(0) = 0 \tag{14}$$

where $\delta < 0$ is a very small constant, e.g., -10^{-6}. The reason for having δ instead of 0 is that the optimization algorithm that we used treats any inequality constraint $w_i \le 0$ as an active constraint, even when $w_i = 0$, and attempts to compute the gradient of w_i. If $\delta = 0$ in Eq. (14), $w_i \le 0$ always will be considered active even if $p_i(\tau) < 0$ for all $\tau \in [0, \tau_f]$. When the algorithm computes the gradient of w_i in this case, it will find that the gradient is zero, which causes premature termination of the optimization process.

The optimization algorithm is a state-of-the-art sequential quadratic programming code developed by Zhou et al.[6] called FFSQP (Fortran Feasible Sequential Quadratic Programming). FFSQP proceeds by first finding a feasible solution that satisfies all of the inequality constraints, if the user-provided initial point is infeasible. Then it generates the successive iterates that all satisfy the inequality constraints. This feature is particularly useful for highly constrained problems such as the current one, where providing a feasible starting point by trial and error is nearly impossible.

For a set of nodal values in the σ-parameterization and the final time τ_f that are now optimization parameters, the trajectory is obtained by numerically integrating Eqs. (1–6). The aerodynamic coefficients C_L and C_D for the X-33, given in tabulated data as functions of Mach number and angle of attack, are found by table lookup. The speed of sound also is found by looking up the data in the 1976 U.S. Standard Atmosphere. The TAEM conditions (7) and inflight constraints (14) constitute the nonlinear equality and inequality constraints of the parameter optimization problem. FFSQP is used to find the optimal parameters that in turn determine the optimal trajectory. Twenty parameters were used, and finite differences were employed for gradient computation. The constraints were satisfied to the accuracy of 10^{-6}.

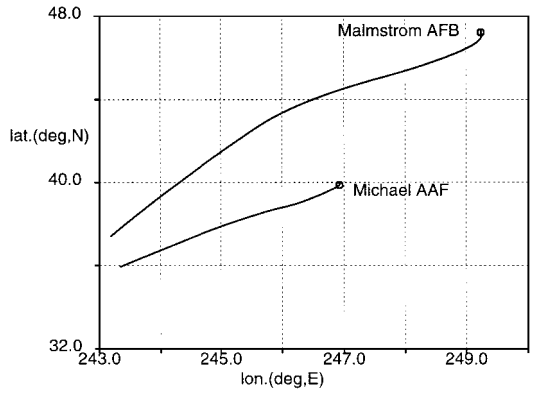

Fig. 1 Ground tracks of the X-33 entry trajectories.

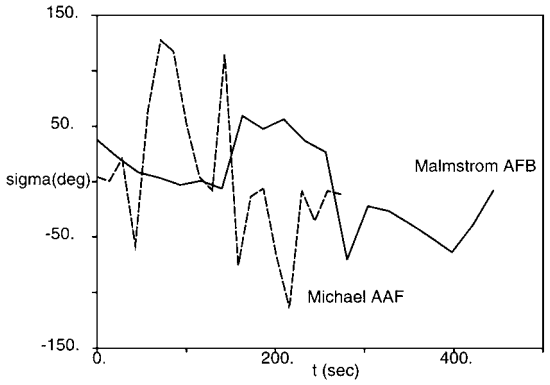

Fig. 2 Bank-angle histories.

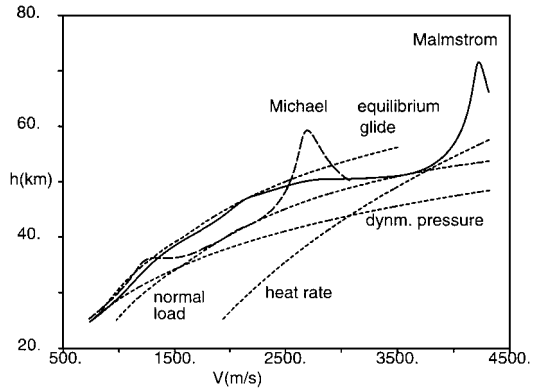

Fig. 3 Entry trajectories to Michael Army Air Field and Malmstrom Air Force Base.

Figure 1 shows the ground tracks of two entry trajectories of the X-33, one with a MECO velocity of Mach 14.2 for landing at Malmstrom Air Force Base in Montana and the other with a MECO velocity of Mach 9.35 for landing at Michael Army Air Field in Utah. The trajectory to Malmstrom Air Force Base has a tight turn at the end to meet a specified azimuth angle condition at TAEM. Figure 2 illustrates the bank-angle histories along the two trajectories. The trajectories in the velocity–altitude space are depicted in Fig. 3 together with the four trajectory constraint boundaries (8–11). Note that the equilibrium glide constraint (11) was not imposed for the trajectory to Michael Army Air Field because it was a relatively short trajectory. A characteristic of the trajectories is that every imposed constraint became active at one point or another, which underscores the importance of these constraints in this problem.

The computation required for these trajectories is very intensive, largely because of the highly constrained nature of the trajectories. Because portions of the trajectories lie on the constraint boundaries, as seen in Fig. 3, the search steps had to be kept small so as not to violate these constraints. With 20 parameters and finite differences for gradient computation, the number of trajectory integrations needed to obtain convergence is on the order of 40,000, which translates into over 10 CPU hours on a DEC 3000/300L Alpha workstation.

Entry Trajectories Defined by Drag Profiles

Nominal Drag Profiles

In Ref. 2, an entry trajectory design method based on piecewise linear parameterization of the drag acceleration profile D with respect to the negative of the dimensionless specific energy

$$e = (1/r) - (V^2/2) \tag{15}$$

is studied. Note that, by its definition, e is monotonically increasing to almost unity along the entry trajectory. It is shown in Ref. 3 that, for a given piecewise linear $D(e)$, the downrange distance traveled by flying this $D(e)$ profile can be predicted accurately by an analytic expression. If it is also desired that the performance index Eq. (12) be minimized as part of the design objectives, a closed-form expression for Eq. (12) as a function of the optimization parameters can be obtained. This approach significantly reduces the difficulty in planning the entry trajectory, handles the trajectory constraints easily, and enables efficient automated nominal entry trajectory generation.

For the convenience of the reader, some of the results in Ref. 3 are reproduced here. Let e_0 and e_f be the prescribed energy levels at MECO and TAEM, respectively. Divide the interval $[e_0, e_f]$ into $n-1$ subintervals by the points $\{e_1, e_2, \ldots, e_n\}$ with $e_1 = e_0$ and $e_n = e_f$. In each interval $[e_i, e_{i+1}]$, $i = 1, \ldots, n-1$, let the desired drag acceleration be parameterized by a linear function of e:

$$D(e) = a_i(e - e_i) + b_i \tag{16}$$

where

$$a_i = \frac{D_{i+1} - D_i}{e_{i+1} - e_i}, \qquad b_i = D_i \tag{17}$$

The values of D_i, $i = 2, \ldots, n-1$, are to be determined. (D_1 and D_n are determined by the MECO and TAEM conditions.) The constraints (8–11) can be expressed in the D-e space as the constraints on D_i:

$$D_{\min}(e_i) \le D_i \le D_{\max}(e_i), \qquad i = 2, \ldots, n-1 \tag{18}$$

If the variation of C_D is ignored, the performance index Eq. (12) can be shown to be proportional to

$$J^* = \int_{e_0}^{e_f} \sqrt{\frac{1-e}{D(e)}}\,\mathrm{d}e = \sum_{i=1}^{n-1} \Delta J_i \tag{19}$$

where

$$\Delta J_i = \begin{cases} (1/a_i)\left[\sqrt{D_{i+1}(1-e_{i+1})} - \sqrt{D_i(1-e_i)}\right] - \left[(a_i + d_i)\Big/\sqrt{a_i^3}\right] \\ \quad \times\left[\tan^{-1}\sqrt{a_i(1-e_{i+1})/D_{i+1}} - \tan^{-1}\sqrt{a_i(1-e_i)/D_i}\right], & a_i > 0 \\ \left(2/3\sqrt{D_i}\right)\left[\sqrt{(1-e_i)^3} - \sqrt{(1-e_{i+1})^3}\right], & a_i = 0 \\ (1/a_i)\left[\sqrt{D_{i+1}(1-e_{i+1})} - \sqrt{D_i(1-e_i)}\right] + \left[(a_i + d_i)\Big/\sqrt{-a_i^3}\right] \\ \quad \times\left[\ln\left|\sqrt{-a_i(1-e_{i+1})} - \sqrt{D_{i+1}}\right| - \ln\left|\sqrt{-a_i(1-e_i)} - \sqrt{D_i}\right|\right], & a_i < 0 \end{cases} \tag{20}$$

The requirement of reaching the TAEM point [$\theta(\tau_f) = \theta_f$ and $\phi(\tau_f) = \phi_f$] is replaced by the requirement that the downrange distance traveled by flying the drag profile be equal to that from MECO to the TAEM point. The downrange distance along the reference trajectory defined by the piecewise linear drag profile Eq. (16) also can be obtained analytically, with the approximation of $\cos\gamma \approx 1$, as

$$s = \sum_{i=1}^{n-1} \Delta s_i \tag{21}$$

where

$$\Delta s_i = \begin{cases} (1/a_i)\ln(D_{i+1}/D_i), & a_i \neq 0 \\ (1/D_i)(e_{i+1} - e_i), & a_i = 0 \end{cases} \tag{22}$$

The design of an optimal entry trajectory now becomes a parameter optimization problem in which the values of the D_i are to be found to minimize J^* in Eq. (19) while satisfying the constraints (18) and

$$\sum_{i=1}^{n-1} \Delta s_i = s_f \tag{23}$$

In this formulation, however, it has been predicted analytically and verified numerically in Ref. 3 that the optimal solution has an undesirable feature of consisting of very rapid changes resulting from inherent discontinuities in the solution of the corresponding variational problem (see Ref. 3 for details). Intuitively, this phenomenon occurs because no vehicle dynamics are directly involved in this optimization process. To add more damping in the $D(e)$ profile, Ref. 3 suggests that a regularization term be included in the cost function to reduce the rate of change of $D(e)$. The cost function for the parameter optimization problem thus becomes

$$\bar{J} = \sum_{i=1}^{n-1} \Delta J_i + \varepsilon \int_{e_0}^{e_f} \left[\frac{\mathrm{d}D(e)}{\mathrm{d}e}\right]^2 \mathrm{d}e$$

$$= \sum_{i=1}^{n-1} \Delta J_i + \varepsilon \sum_{i=1}^{n-1} \left[\frac{(D_{i+1} - D_i)^2}{e_{i+1} - e_i}\right] \tag{24}$$

where $\varepsilon > 0$ is a small constant ($\varepsilon = 5 \times 10^{-6}$ in this study). For the X-33, it is necessary to specify the first three nodes D_1, D_2, and D_3 to match the MECO condition and reflect the ascent of the trajectory immediately after MECO. (Otherwise, the optimal drag profile will call for a descent trajectory right from MECO, which is not flyable because γ is still positive at MECO.)

Because no numerical integrations are required and the trajectory constraints are handled by the box constraints (18), the optimization problem can be solved much more efficiently as compared to the trajectory optimization approach in the preceding section. For the same number of parameters (20) and with the use of finite differences for gradient computation (although not necessary in this case, because the analytical formulas are available), the typical number of function evaluations is on the order of 1500. The CPU time spent on the same DEC Alpha workstation is only about 30 s.

Figure 4 shows the comparison of the drag profile obtained here (in solid line) with the drag acceleration variation in dashed line along the numerical optimal trajectory shown in Fig. 3 for landing at Malmstrom Air Force Base. The piecewise linear drag profile clearly captures the essential features of the numerical optimal solution at a small computation cost. The important difference at this point is that the numerical optimal trajectories can be designed at the expense of intensive computation to exactly meet the conditions for $\gamma(\tau_f)$ and $\psi(\tau_f)$ at TAEM. In contrast, the heading control along the trajectory defined by the drag profile has to be obtained by bank-angle reversals,[1] and no direct control over $\gamma(\tau_f)$ is implemented, although an appropriately scheduled nominal α-program can result in a $\gamma(\tau_f)$ in the allowable range. Accurate satisfaction of the TAEM condition on $\psi(\tau_f)$, when required, is to be achieved by a technique that is discussed in the later section on pre-TAEM trajectory control.

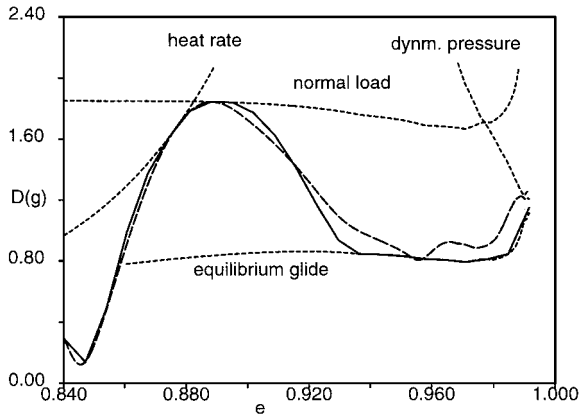

Fig. 4 Comparison of drag profiles for landing at Malmstrom: ——, piecewise linear $D(e)$, and – – –, along the trajectory in Fig. 3.

The chief benefits of the current approach are that the nominal entry trajectory can be designed very effectively, reliably, and quickly, and the design process can be automated easily, thus saving significant amount of time and manpower. This feature probably is particularly useful for an evolving test vehicle such as the X-33.

Drag Profile Update

In the actual flight, downrange error between the predicted and true ranges will occur because of a number of factors such as the rotation of Earth, lateral motion of the vehicle, inaccuracy in tracking the nominal drag profile, and modeling uncertainties. The Shuttle entry guidance system adjusts onboard one segment of the nominal drag profile at a time to null the range error.[1] The principle is to use the analytical downrange distance expression and a first-order Taylor-series expansion of the expression to determine the amount of the adjustment. Because we have used much shorter (therefore more) segments to define the drag profile, adjusting only one segment at a time to null the range error tends to require relatively large perturbation in that segment. The validity of the first-order expansion in such a case is questionable and the effectiveness of the update is usually poor. Hence, we adjust k nodes of the drag profile at a time for some $k \geq 1$, provided that there are still no less than k adjustable nodes ahead along the trajectory as the flight progresses.

Suppose that, at the instant of updating, the current energy e is between $[e_i, e_{i+1}]$, and the difference between the range-to-go predicted by the analytical Eqs. (21) and (22) and the actual range-to-go is δs. To null the error δs, the nodes $D_{i+1}, \ldots, D_{i+k}$ are to be adjusted. Let the perturbations for the nodes be $\delta D_{i+1}, \ldots, \delta D_{i+k}$. The first-order expansion of the range-to-go is then

$$\delta s = \left(\frac{\partial \Delta s_i}{\partial D_{i+1}} + \frac{\partial \Delta s_{i+1}}{\partial D_{i+1}}\right)\delta D_{i+1} + \cdots$$

$$+ \left(\frac{\partial \Delta s_{i+k-1}}{\partial D_{i+k}} + \frac{\partial \Delta s_{i+k}}{\partial D_{i+k}}\right)\delta D_{i+k} \triangleq \boldsymbol{c}^T \delta \boldsymbol{D} \tag{25}$$

where all of the partial derivatives are analytically evaluated and $\delta \boldsymbol{D} = (\delta D_{i+1}, \ldots, \delta D_{i+k})^T$. Equation (25) admits infinitely many solutions when $k > 1$, but the minimum-norm solution, which is the one with the smallest $\|\delta \boldsymbol{D}\|^2 = \delta \boldsymbol{D}^T \delta \boldsymbol{D}$, is given by

$$\delta \boldsymbol{D} = (\delta s / \boldsymbol{c}^T \boldsymbol{c})\, \boldsymbol{c} \tag{26}$$

The updated values of the nodes $D_{i+1}, \ldots, D_{i+k}$ then are given by $D_{i+1} + \delta D_{i+1}, \ldots,$ and $D_{i+k} + \delta D_{i+k}$. The updated piecewise linear drag profile thus is obtained.

For the current X-33 applications, we have found that $k = 3$ and updating the drag profile once every 5 s suffice. Increasing k beyond 3 does not seem to offer further noticeable improvement. Also, to ensure the validity of linearization (25), each δD_{i+j}, $1 \leq j \leq k$, should be limited to a maximum magnitude, when $|\delta D_{i+j}|$ given by Eq. (26) is greater than that limit. A limit of 1% of D_{i+j} is used in this work, although values such as 2 and 3% give comparable results.

Trajectory Control

Drag-Profile Tracking Control Law

The Space Shuttle employs a time-varying, linearized trajectory control law for tracking the nominal drag profile during entry flight.[1] The gains of the control law are scheduled for different regimes of the flight. These gains are trajectory specific, and their tuning is time-consuming. Because the vehicle dynamics are inherently nonlinear and the flight conditions during the entry are widely different, nonlinear control methods appear to be well suited for trajectory control law design. Such a possibility is demonstrated[7] with a feedback linearization control law. More recently, a nonlinear predictive control law[3] has been used for entry trajectory tracking control. In this approach, denoting $u = C_L \cos\sigma / C_D$, we can express

$$\ddot{D} = a_D + b_D u \tag{27}$$

where a_D and b_D are functions of r, V, γ, and D, which can be obtained readily from the definition of D and Eqs. (1) and (4), if we ignore the rotation of Earth, $\dot{C}_D$, and $\ddot{C}_D$. Furthermore, $b_D \neq 0$ for all $V > 0$ and $|\gamma| < 90$ deg. Let $\Delta D = D - D^*$, with D^* representing the reference drag acceleration. Define an auxiliary variable

$$z(\tau) = \Delta\dot{D} + 2\zeta\omega_n \Delta D + \omega_n^2 \int_0^\tau \Delta D(\mu)\, \mathrm{d}\mu \tag{28}$$

where $\zeta > 0$ and $\omega_n > 0$ are two constants, the meaning of which will be clear shortly. By its definition, z is a first-order variable with respect to u because $\dot{z}$ depends on u explicitly. Hence the influence of $u(\tau)$ on $z(\tau + T)$ for a time increment $T > 0$ can be predicted by a first-order Taylor-series expansion

$$z(\tau + T) \approx z(\tau) + T\dot{z}(\tau) = z(\tau) + T\left[a_D(\tau) + b_D(\tau)u(\tau) + 2\zeta\omega_n \Delta\dot{D}(\tau) + \omega_n^2 \Delta D(\tau) - \ddot{D}^*(\tau)\right] \tag{29}$$

where, for the piecewise linear parameterization of D^* with respect to e, we have in the interval $[e_i, e_{i+1}]$

$$\dot{D}^* = a_i DV, \qquad \ddot{D}^* = a_i(\dot{D}V + D\dot{V}) \tag{30}$$

where a_i is from Eq. (17). Note that, for accurate tracking of D^*, we desire that $z \to 0$. To find the control u for this purpose, consider the minimization of the performance index

$$J = \tfrac{1}{2} z^2(\tau + T) \tag{31}$$

at an arbitrary $\tau \in [0, \tau_f)$. Replacing $z(\tau + T)$ by Eq. (29) and setting $\partial J / \partial u(\tau) = 0$ gives a continuous, nonlinear feedback control law

$$u(\tau) = -(1/Tb_D)\left[z + T\left(a_D - \ddot{D}^* + 2\zeta\omega_n \Delta\dot{D} + \omega_n^2 \Delta D\right)\right] \tag{32}$$

Globally asymptotically stable tracking of D^* for any $T > 0$ under this control law can be seen by substituting Eq. (32) into the equation for $\dot{z}$ to arrive at

$$\dot{z} = -(1/T)z \tag{33}$$

Thus $z \to 0$ exponentially with a time-constant T, and $\dot{z} \to 0$, provided that no control saturation is encountered. From the definition of z, $\dot{z} = 0$ leads to

$$\Delta\ddot{D} + 2\zeta\omega_n \Delta\dot{D} + \omega_n^2 \Delta D = 0 \tag{34}$$

Therefore, $\Delta D \to 0$ with a damping ratio of ζ and natural frequency of ω_n. For the X-33 applications, we have chosen $\zeta = 0.7$, $T = 0.01\sqrt{(R_0/g_0)}$ (s), and $\omega_n = 0.04\sqrt{(R_0/g_0)}$, or $1/\omega_n$ corresponds to 25 s in real time.

From the definition of z in Eq. (28), it is clear that Eq. (32) defines a nonlinear proportional-plus-integral-plus-derivative control law. The only parameters to be selected are T, ζ, and ω_n, and no other gains need be tuned. Once the three parameters are chosen, no additional gain scheduling or onboard storage of massive data along the nominal trajectory is required when a piecewise linear $D^*(e)$ is used. Note that T does not have to be small for the asymptotic tracking to hold even though it is originally introduced as a time step in the Taylor-series expansion Eq. (29). With u determined by Eq. (32), the magnitude of the commanded bank angle σ_{com} for trajectory tracking is computed from $\cos\sigma_{\text{com}} = uC_D/C_L$. The cross range is controlled by reversals of the orientation of the bank angle. Suppose that ψ^* is the azimuth pointing from the current position toward the TAEM point. When the magnitude of the azimuth error $\Delta\psi = \psi - \psi^*$ exceeds a dead-band limit, the bank angle is reversed to the opposite direction to reduce $\Delta\psi$.

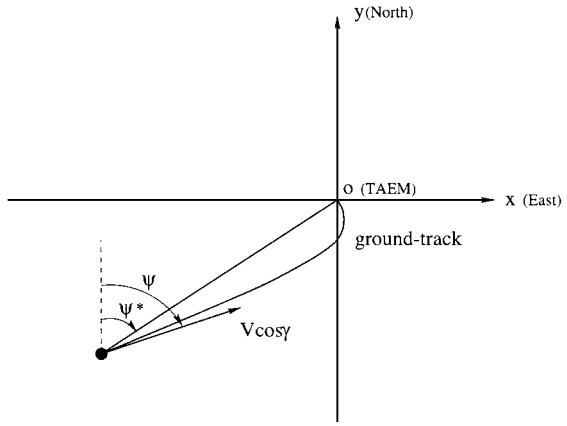

Fig. 5 Coordinate system for final ground-track planning.

Pre-TAEM Ground-Track Control

When the vehicle reaches the TAEM point by following the designed drag profile, the final heading will take whatever value the trajectory naturally leads to. This heading can be far from the desired direction, especially when the vehicle is required to approach the TAEM point from a specified direction that is not natural for the entry trajectory. For instance, when the X-33 lands at the Malmstrom Air Force Base, the entry flight is from southwest to northeast (cf. Fig. 1), but in an early design, the X-33 is required to approach the TAEM point from southeast to avoid a populated area. In situations such as this, additional measures need to be taken to satisfy the heading condition at the TAEM interface. One possibility is for the guidance system to control the vehicle to follow an appropriately designed ground track once the vehicle is near TAEM, instead of tracking the drag profile. In the following, we discuss a method for this purpose.

Use flat-earth assumption in this phase. Let oxy be a coordinate system centered at the TAEM point with the y axis pointing to the north, and the x axis to the east, as shown in Fig. 5. The kinematics of the vehicle in the horizontal plane are

$$\dot{x} = V\cos\gamma\sin\psi \tag{35}$$

$$\dot{y} = V\cos\gamma\cos\psi \tag{36}$$

From these two equations, we have

$$\frac{\mathrm{d}x}{\mathrm{d}y} = \tan\psi \tag{37}$$

The desired ground track is chosen to be a cubic curve

$$x = ay^3 + by^2 + cy \tag{38}$$

where the coefficients a, b, and c are to be determined. Suppose that, at the instant τ_0 when the tracking of the ground track begins, $x(\tau_0) = x_0$ and $y(\tau_0) = y_0$, and the line-of-sight angle from the vehicle to the TAEM point is ψ_0^*. Also, the azimuth angle required at the TAEM interface is given as ψ_d. First, we set $c = \tan\psi_d$. Then, along Eq. (38) at the TAEM point where $x = y = 0$,

$$\left.\frac{\mathrm{d}x}{\mathrm{d}y}\right|_{x=y=0} = \tan\psi(\tau_f) = c = \tan\psi_d \tag{39}$$

Thus $\psi(\tau_f) = \psi_d$. The coefficients a and b are found by satisfying

$$x_0 = ay_0^3 + by_0^2 + cy_0 \tag{40}$$

$$\left.\frac{dx}{dy}\right|_{\tau=\tau_0} = 3ay_0^2 + 2by_0 + c = \tan\psi_0^* \tag{41}$$

Condition (40) means that the desired ground track, Eq. (38), starts at the current point; Eq. (41) specifies that the ground track points directly toward the TAEM point (origin) at the beginning. This condition is important because, with Eq. (41), the desired ground track conforms with the general direction of motion of the vehicle; thus the ground track is achievable by the vehicle. The solution to these two equations is

$$a = -\frac{2(x_0 - y_0\tan\psi_d) - y_0\left(\tan\psi_0^* - \tan\psi_d\right)}{y_0^3} \tag{42}$$

$$b = \frac{3(x_0 - y_0\tan\psi_d) - y_0\left(\tan\psi_0^* - \tan\psi_d\right)}{y_0^2} \tag{43}$$

Now, by following the ground track, Eq. (38), with the coefficients defined in Eqs. (39), (42), and (43), the vehicle will reach the TAEM point at $x = y = 0$ with $\psi(\tau_f) = \psi_d$. This ground track can be easily designed onboard, given the navigation information on x_0, y_0, and ψ_0^*.

Next, we derive the bank-angle control law to track Eq. (38). To avoid differentiation of γ, which involves the term $\cos\sigma$ and thus makes it difficult to obtain a closed-form control law, we introduce a new independent variable ξ

$$\xi = \int_{\tau_0}^{\tau} V(\nu)\cos\gamma(\nu)\,d\nu \tag{44}$$

or

$$d\xi = V\cos\gamma\,d\tau \tag{45}$$

Therefore, the kinematic equations (35) and (36) become

$$x' = \sin\psi \tag{46}$$

$$y' = \cos\psi \tag{47}$$

where the prime stands for differentiation with respect to ξ. Let

$$F = x - ay^3 - by^2 - cy \tag{48}$$

Thus,

$$F' = \sin\psi - 3ay^2\cos\psi - 2by\cos\psi - c\cos\psi \tag{49}$$

$$F'' = [\cos\psi + (3ay^2 + 2by + c)\sin\psi]\psi'$$

$$-(6ay + 2b)\cos^2\psi \triangleq A_F\psi' + B_F \tag{50}$$

where, from Eq. (6) with the Earth's rotation ignored and Eq. (45), we have

$$\psi' = \dot{\psi}/V\cos\gamma = (L/V^2\cos^2\gamma)\sin\sigma$$

$$+ V\sin\psi\tan\phi/r \triangleq G_\psi\sin\sigma + H_\psi \tag{51}$$

Choose a feedback linearization control law

$$\sin\sigma = \frac{-A_F H_\psi - B_F - 2\zeta_F\omega_{n_F}F' - \omega_{n_F}^2 F}{A_F G_\psi} \tag{52}$$

where $\zeta_F > 0$ and $\omega_{n_F} > 0$ are two constants. Substituting Eqs. (51) and (52) into Eq. (50) gives the closed-loop dynamics

$$F'' + 2\zeta_F\omega_{n_F}F' + \omega_{n_F}^2 F = 0 \tag{53}$$

It follows that $F \to 0$, or $x = ay^3 + by^2 + cy$, asymptotically.

Remarks:

1) The new variable ξ is introduced only to enable us to derive the closed-form control law. The control law, Eq. (52), is a function of the position coordinates and other states, independent of ξ.

2) Note that ω_{n_F} is the natural frequency in ξ, not in the real time t or dimensionless time τ. So, the value of ω_{n_F} may not have exactly the same influence on the transient tracking response in the real time, but it still should have qualitatively similar effects. The steady-state response $F = 0$ is the same, which is what we desire.

3) The guidelines for selecting ω_{n_F} and, to a lesser extent, ζ_F, are such that a) the control law Eq. (52) is not severely saturated and b) the vehicle reaches the TAEM point with an acceptable energy level. For the entry flight of the X-33 to Malmstrom Air Force Base tested in the "Simulations" section, we have used $\zeta_F = 0.7$ and $\omega_{n_F} = 350$, which corresponds to a dimensional natural frequency of $350/\sqrt{(R_0/g_0)} = 0.434$ (1/s).

4) The starting point of the ground-track control phase may differ, depending on how hard the vehicle needs to maneuver to meet the final heading condition. In general, it should be initiated as close to TAEM as possible to ensure that the vehicle reaches TAEM with proper energy. For the X-33 landing at Malmstrom Air Force Base, the difference between the required azimuth angle and the natural one is over 40 deg in our simulations. Hence the ground-track control is initiated at a distance of 150 km (at about Mach 5.2) from the TAEM interface to allow enough time for the maneuver.

5) When the ground track, Eq. (38), is followed, the vehicle is guaranteed within the accuracy of the analysis to reach the TAEM point because the ground track, Eq. (38), passes through the TAEM point, whether or not there is a range error at τ_0. Therefore, this feature is expected to improve the overall performance of the guidance algorithm in trajectory dispersion study. When the final ground-track control is employed, the updating of the drag profile discussed earlier serves more the purpose of keeping the trajectory at correct energy level than eliminating the range error. See the discussion of the numerical results in the "Simulations" section.

6) Even when the final heading of the entry trajectory is not required to meet a strict condition, the ground-track control still can be employed to achieve precise TAEM point location. In this case, ψ_d simply can be set equal to ψ_0^*. Then, $a = b = 0$ by Eqs. (42) and (43), and the reference ground track, Eq. (38), degenerates to a straight line. The vehicle will follow this straight line to the TAEM point. This usually is a much less aggressive maneuver for the vehicle compared to the case in which a specified final heading is required.

Although the control law, Eq. (52), controls the lateral motion of the vehicle, the longitudinal motion needs to be monitored so that the trajectory constraint $\bar{q} \le \bar{q}_{\max}$ in this phase is not violated. To this end, the angle of attack α is modulated in this period according to

$$\alpha = \alpha_{\text{ref}} + \alpha_q e^{-k_q(1-\bar{q}/\bar{q}_{\max})} \tag{54}$$

where $\alpha_q > 0$ and $k_q > 0$ are two selected constants. Appropriate values for α_q and k_q will result in $\alpha \approx \alpha_{\text{ref}}$ when $\bar{q}$ is away from and less than $\bar{q}_{\max}$, and α will increase as $\bar{q} \to \bar{q}_{\max}$. As a result, the altitude decrease will slow and $\bar{q} < \bar{q}_{\max}$ will remain enforced. For our X-33 applications, $\alpha_q = 10$ deg and $k_q = 10$, among many other possible combinations, appear to work well.

Trajectory Control Logic for the X-33

Before applying the control laws obtained in the preceding sections to the X-33, we make the following observation. Take the flight to Malmstrom Air Force Base as an example. In the altitude range between 55 and 70 km, the velocity of the X-33 is about 70% of the velocity of a vehicle returning from orbit. Thus, the aerodynamic control authority of the X-33 is only 50% of what an orbital vehicle would have, everything else being equal. This reduction would result in very large control (bank-angle) excursions and often saturation if closed-loop control is used in this altitude range, and the trajectory-tracking performance would be poor. For an orbital vehicle, the entry trajectory control is activated after the dynamic pressure has increased to a threshold level. For the X-33, because of the ascent–descent feature of the trajectory, the dynamic pressure variation is not monotonic. More important, it was found that some trajectory shaping has to be performed during the ascent after MECO to avoid violating the normal acceleration and/or heat rate constraints, Eqs. (8) and (10), in the subsequent descent, even if the dynamic

pressure is low in this ascent period. It is particularly the case for landing at Malmstrom Air Force Base. To address these problems, an alternative is to use open-loop control initially and switch to closed-loop control after sufficient aerodynamic control is available.

Consider the entry flight of the X-33 to Malmstrom Air Force Base. Following the preceding discussion, we first use $\sigma_{\text{com}} = 40$ (deg) in the ascent from MECO until $\gamma = 0$. Using $\sigma \neq 0$ in this phase tends to flatten the ascent trajectory so that the subsequent descent will not be as steep. From the highest point of the trajectory to the point of $e = 0.89$, where approximately the maximum normal load is reached, $\sigma_{\text{com}} = 0$ is used. This bank angle places all of the lift in the vertical plane so that the descending trajectory will be relatively shallow; therefore, the normal load and heat rate constraints (8) and (10) will be observed. From the point where $e = 0.89$ on, σ_{com} is computed from the nonlinear feedback control law, Eq. (32), until the vehicle is 150 km away from the TAEM, after which point the ground-track control law, Eq. (52), is applied. In summary, the trajectory control logic for entry flight to Malmstrom Air Force Base is

$$\sigma_{\text{com}} = \begin{cases} 40 \text{ deg}, & \text{in ascent following MECO} \\ 0, & \text{from } \gamma = 0 \text{ to } e = 0.89 \\ \text{Eq. (32)}, & 0.89 \leq e \text{ and distance to TAEM} > 150 \text{ km} \\ \text{Eq. (52)}, & \text{distance to TAEM} \leq 150 \text{ km} \end{cases} \tag{55}$$

The choice of 40 deg is not critical. Other magnitudes ranging from 30 to 80 deg would give a very close result. The control logic can be modified to adapt to different MECO conditions for entry flight to other landing sites, e.g., Michael Army Air Field.

To smooth out the jumps in σ_{com} caused by the slope discontinuities in the piecewise linear D^* profile and the control logic switchings, the actual bank angle σ is obtained as the output of a filter

$$\dot{\sigma} = -(1/T_\sigma)(\sigma - \sigma_{\text{com}}) \tag{56}$$

where $T_\sigma = 0.005\sqrt{(R_0/g_0)}$ (s) is selected. The obtained σ is used in the general equations of motion (1–6) for numerical simulation of the trajectory. A dead band of ± 10 deg in heading error $\Delta\psi$ is used for determining bank reversals for σ_{com} computed from Eq. (32).

Simulations

In this section we numerically test the techniques discussed earlier. The initial conditions are the MECO conditions obtained from early X-33 trajectory designs. The entry trajectories are obtained by numerically integrating Eqs. (1–6) with the bank angle determined from Eq. (55) and C_L and C_D found by table lookup of early X-33 aerodynamic data. The simulation of the entry trajectory is terminated when the energy reaches the required level.

Three drag profiles for the X-33 landing at Malmstrom Air Force Base are plotted in Fig. 6. The dotted line is the nominal piecewise linear D^* also shown as the solid line in Fig. 4. The solid line in Fig. 6 is the drag variation under the control logic Eq. (55), except for the last-phase ground-track control. The dashed line represents the drag profile under the same control logic, but with the reference drag profile updated every 5 s beginning at $e = 0.89$, where the tracking control law, Eq. (32), is applied. It can be seen that Eq. (32) tracks the nominal drag profile well, and the drag update has an obvious effect on the trajectory. Table 1 lists some corresponding TAEM conditions for several trajectories: trajectory 1, serving as the benchmark, is the numerical optimal trajectory, and the ground track is shown in Fig. 1; trajectory 2 is the one without drag-profile update and final ground-track control (solid line in Fig. 6); trajectory 3 is the one with drag-profile update but no ground-track control (dashed line in Fig. 6); and trajectory 4 is a trajectory that uses the drag update scheme and the control logic (55), including the final ground-track control law (52). The quantity d_f in Table 1 stands for the distance to the given TAEM point at the end of the trajectory.

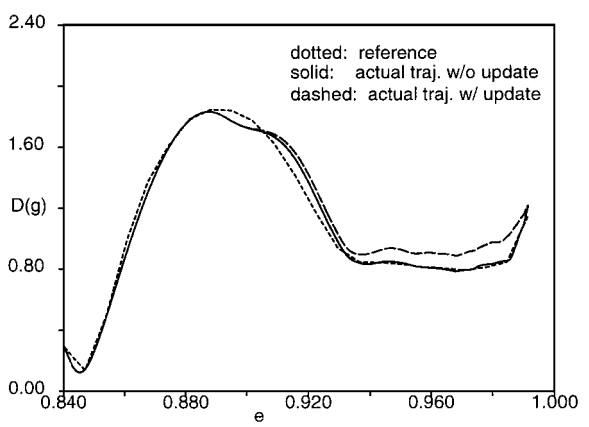

Fig. 6 Comparison of drag profiles for landing at Malmstrom with and without drag profile update.

The trajectory control law (32) tracks the reference drag profile closely, but without drag updating, the trajectory misses the TAEM point by 47.6 km (trajectory 2). With drag updating, the miss distance is reduced to only 1.86 km (trajectory 3), but the problem now is with the final azimuth angle ψ_f, which is 36.6 deg, far from the required -5.14 deg. Adding the previously developed ground-track control phase effectively corrects this problem and further reduces the miss distance, yielding $\psi_f = -5.75$ deg and $d_f = 0.18$ km (trajectory 4).

Figure 7 compares the bank-angle histories of trajectories 3 and 4. The difference is only in the last 100 s or so, when the ground-track control is applied. Comparison of the nominal angle of attack and the actual angle of attack along trajectory 4 is shown in Fig. 8. The

Table 1 Comparison of TAEM conditions for landing at Malmstrom Air Force Base

Trajectory	d_f, km	h_f, km	V_f, m/s	ψ_f, deg	γ_f, deg
1	0	24.75	740.00	−5.14	−11.0
2	47.57	24.70	739.90	−2.34	−16.3
3	1.86	24.66	740.65	36.63	−14.6
4	0.18	25.52	730.0	−5.75	−8.6

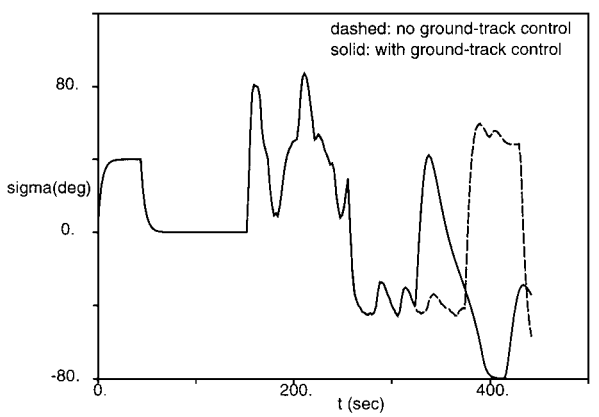

Fig. 7 Bank-angle histories for the X-33 landing at Malmstrom.

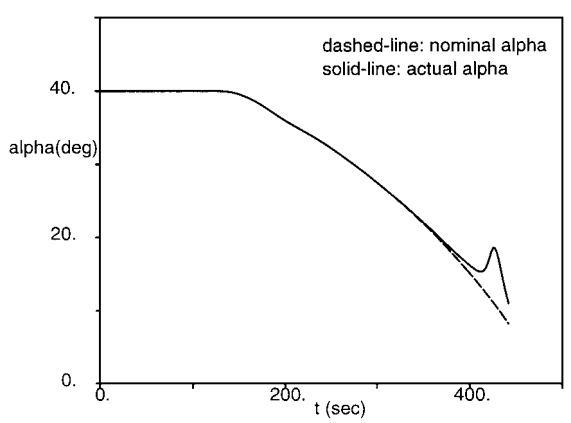

Fig. 8 Angle of attack of the X-33 landing at Malmstrom.

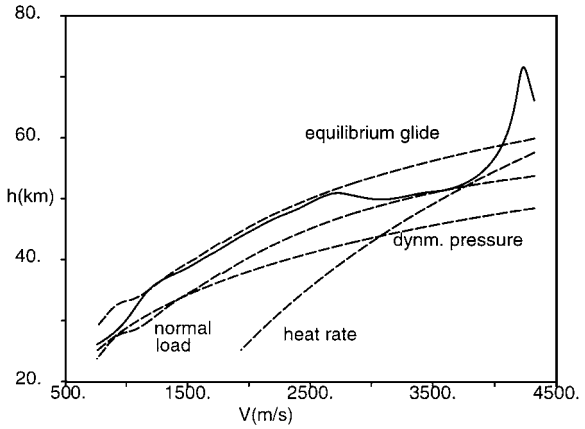

Fig. 9 Entry trajectory to Malmstrom generated by tracking the piecewise linear drag profile and controlling the pre-TAEM ground track.

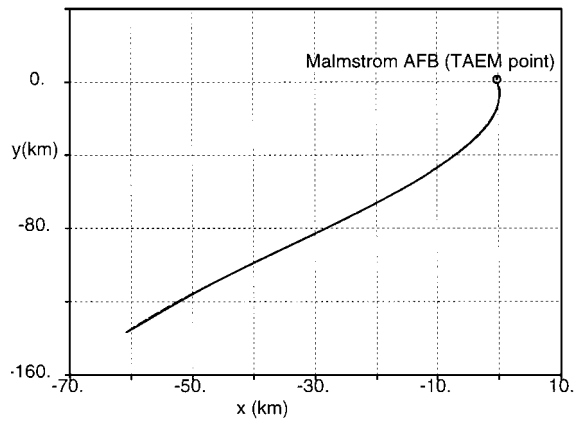

Fig. 10 Comparison of ground tracks: – – –, desired [Eq. (38)], and ——, actual.

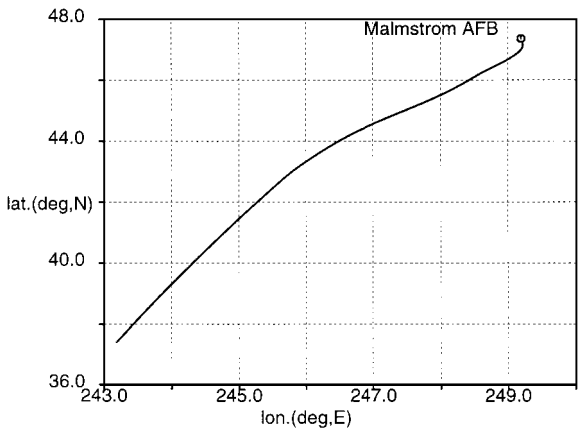

Fig. 11 Ground track of the X-33 landing at Malmstrom.

visible small hump near the end is due to the angle-of-attack modulation, Eq. (54), when the trajectory moves closer to the boundary of $\bar{q} \leq \bar{q}_{\max}$. Figure 9 shows trajectory 4 (solid line) in the velocity-altitude space with the constraint boundaries of Eqs. (8–11). Clearly, all of the constraints are met and the trajectory looks similar to trajectory 1, which is plotted in Fig. 3 as a solid line. Without the angle-of-attack modulation, Eq. (54), the constraint $\bar{q} \leq \bar{q}_{\max}$ would have been violated in this case.

The desired ground track equation (38) for trajectory 4 and the actual ground track starting at a distance of 150 km from the TAEM point are illustrated in Fig. 10. The tracking is so good that the two tracks are virtually indistinguishable at the scale shown. Figure 11 shows the complete ground track of trajectory 4. Again, the ground track is very similar to the one along the optimal solution plotted in Fig. 1 (trajectory 1).

Finally, we applied the control logic, Eq. (55), without updating the drag profile. Although the ground-track control law was able to lead the vehicle to the TAEM point with correct heading. Despite the range error, the energy of the vehicle was excessive compared to the specified value; the final velocity was 855.4 m/s and the altitude 27.72 km. Therefore, the updating of the drag profile helps the vehicle to maintain proper energy level even though the final ground-track control phase can effectively eliminate the range error.

Conclusions

The approach to designing the entry trajectory by way of a drag profile that is piecewise linear in specific energy appears to be well suited for the entry guidance of the X-33 vehicle. Such an optimized drag profile captures to a remarkable extent the essential aspects of the trajectory obtained by solving a computationally intensive trajectory optimization problem with full three-dimensional equations of motion. With a nonlinear tracking control law for the bank angle and appropriate periodic update of the reference drag profile, the vehicle is guided to the designated TAEM point with good accuracy. When the vehicle heading at the TAEM point is required to meet a stringent condition and/or precise arrival at the TAEM point is desired, a final-phase ground-track control method is developed. In such a case, a desired ground track passing through the TAEM point with the specified heading angle is designed onboard at a distance before TAEM, and a nonlinear bank-angle control law is derived to track the desired ground track. Combining the nominal trajectory design technique and the nonlinear trajectory control laws with an open-loop scheme for initial trajectory control, the approach offers a fast, effective, and automated entry guidance algorithm for the X-33 that has the potential to perform well both offline and onboard. An important aspect of the entry guidance study—trajectory dispersion analysis—has not yet been performed. Our expectation, which remains to be verified, is that the algorithm should be quite robust because of the drag-updating scheme, the ground-track following maneuver, and the expected robustness of the nonlinear trajectory control laws.

Acknowledgment

This research has been supported by NASA Marshall Space Flight Center under Grant NAG8-1289.

References

[1] Harpold, J. C., and Graves, C. A., "Shuttle Entry Guidance," *Journal of the Astronautical Sciences*, Vol. 37, No. 3, 1979, pp. 239–268.

[2] Roenneke, A. J., and Markl, A., "Re-Entry Control of a Drag vs Energy Profile," *Journal of Guidance, Control, and Dynamics*, Vol. 17, No. 5, 1994, pp. 916–920.

[3] Lu, P., "Entry Guidance and Trajectory Control for Reusable Launch Vehicle," *Journal of Guidance, Control, and Dynamics*, Vol. 20, No. 1, 1997, pp. 143–149.

[4] Vinh, N. X., Busemann, A., and Culp, R. D., *Hypersonic and Planetary Entry Flight Mechanics*, Univ. of Michigan Press, Ann Arbor, MI, 1980, pp. 26, 27.

[5] Regan, F. J., and Anandakrishnan, S. M., *Dynamics of Atmospheric Reentry*, AIAA Education Series, AIAA, Washington, DC, 1993, p. 38.

[6] Zhou, J. L., Tits, A. L., and Lawrence, C. T., "User's Guide for FFSQP Version 3.7: A Fortran Code for Solving Constrained Nonlinear (Minimax) Optimization Problems, Generating Iterates Satisfying all Inequality and Linear Constraints," Systems Research Center, TR-92-107r2, Univ. of Maryland, College Park, MD, April 1997.

[7] Mease, K. D., and Kremer, J.-P., "Shuttle Guidance Revisited Using Nonlinear Geometric Methods," *Journal of Guidance, Control, and Dynamics*, Vol. 17, No. 6, 1994, pp. 1350–1356.

F. H. Lutze Jr.
Associate Editor